



HAL
open science

High-Efficiency Ion-Exchange Doping of Conducting Polymers

Ian E Jacobs, Yue Lin, Yuxuan Huang, Xinglong Ren, Dimitrios Simatos, Chen Chen, Dion Tjhe, Martin Statz, Lianglun Lai, Peter A Finn, et al.

► **To cite this version:**

Ian E Jacobs, Yue Lin, Yuxuan Huang, Xinglong Ren, Dimitrios Simatos, et al.. High-Efficiency Ion-Exchange Doping of Conducting Polymers. *Advanced Materials*, 2021, 34 (22), pp.2102988. 10.1002/adma.202102988 . hal-03411915

HAL Id: hal-03411915

<https://hal.science/hal-03411915>

Submitted on 4 Nov 2021

HAL is a multi-disciplinary open access archive for the deposit and dissemination of scientific research documents, whether they are published or not. The documents may come from teaching and research institutions in France or abroad, or from public or private research centers.

L'archive ouverte pluridisciplinaire **HAL**, est destinée au dépôt et à la diffusion de documents scientifiques de niveau recherche, publiés ou non, émanant des établissements d'enseignement et de recherche français ou étrangers, des laboratoires publics ou privés.

High efficiency ion exchange doping of conducting polymers

Ian E. Jacobs,¹ Gabriele D'Avino,² Yue Lin,¹ Vincent Lemaire,³ Yuxuan Huang,¹
Xinglong Ren,¹ Dimitrios Simatos,^{1,4} Chen Chen,¹ Dion Tjhe,¹ Martin Statz,¹
Lianglun Lai,¹ Peter A. Finn,⁵ William G. Neal,⁵ Joseph Strzalka,⁷ Christian B. Nielsen,⁵
Stephen Barlow,⁷ Seth R. Marder,⁷ Iain McCulloch,^{8,9} Simone Fratini,² David Beljonne,³
³ Henning Sirringhaus¹

April 16, 2021

¹ Optoelectronics Group, Cavendish Laboratory, University of Cambridge, J J Thomson Avenue, Cambridge CB3 0HE, UK ² Grenoble Alpes University, CNRS, Grenoble INP, Institut Néel, 25 rue des Martyrs, 38042 Grenoble, France ³ Laboratory for Chemistry of Novel Materials, University of Mons, Mons, B-7000 Belgium ⁴ Department of Chemistry, University of Cambridge, Lensfield Road, Cambridge, CB2 1EW, UK ⁵ School of Biological and Chemical Sciences, Queen Mary University of London, Mile End Road, London, E1 4NS, UK ⁶ X-Ray Science Division, Argonne National Laboratory, Lemont, IL, 60439 USA ⁷ School of Chemistry and Biochemistry and Center for Organic Photonics and Electronics, Georgia Institute of Technology, Atlanta, Georgia 30332, United States ⁸ KAUST Solar Center, Physical Sciences and Engineering Division (PSE), Materials Science and Engineering Program (MSE), King Abdullah University of Science and Technology (KAUST), Thuwal, Kingdom of Saudi Arabia ⁹ Department of Chemistry, University of Oxford, Oxford, UK

Abstract

Molecular doping—the use of redox-active small molecules as dopants for organic semiconductors—has seen a surge in research interest driven by emerging applications in sensing, bioelectronics and thermoelectrics. However, molecular doping carries with it several intrinsic problems stemming directly from the redox-active character of these materials. A recent breakthrough was a doping technique based on ion-exchange, which separates the redox and charge compensation steps of the doping process. Here, we study the equilibrium and kinetics of ion exchange doping in a model system, PBTTT doped with FeCl₃ and BMP TFSI, which reaches conductivities in excess of 1000 S/cm and ion exchange efficiencies above 99%. We demonstrate several factors which enable such high performance, including the choice of acetonitrile as the doping solvent, which largely eliminates electrolyte association effects and dramatically increases the doping strength of FeCl₃. In this high ion exchange efficiency regime, we illustrate a simple connection between electrochemical doping and ion exchange, and show that the performance and stability of highly doped PBTTT is ultimately limited by intrinsically poor stability at high redox potential.

Introduction

The simplest, most common approach to doping in semiconducting polymers, molecular doping[1, 2, 3] (Figure 1a) has several fundamental limitations. These arise from the requirement that the dopant molecule must perform two seemingly unrelated roles. In p-type doping, initially the dopant functions as an oxidizing agent, nearly always via a reversible electron transfer reaction, the product of which is then inserted as an ionized dopant into the film to compensate the positive charge on the polymer. Requiring a single chemical species to perform both these functions leads to several difficulties:

1. P-type dopants are by definition strong electrophiles, and thus quite reactive.[4, 5, 2] Because at equilibrium a small population of neutral dopants always exists, both redox states of the dopant need to be chemically inert. This puts hard constraints on suitable molecular dopants.
2. The electron affinity of many dopants is significantly reduced when incorporated into an organic semiconductor[6] making it difficult to predict whether a given polymer and dopant molecule will undergo charge-transfer.
3. When the electron transfer step is reversible, the dopant ion is inherently redox-active; p-type dopants therefore will almost always have electronic states in close vicinity to those of the polymer (Figure 1d).[7, 1] In polymers there is growing evidence that integer charge-transfer is stabilized by the segregation of dopant ions to the sidechain region, where π -orbital overlap with the polymer is minimized.[8, 9, 10] In contrast, when the dopant does π -stack with the polymer, fractional charge-transfer complex (CTC) formation is observed.[11] Therefore, fractional CTCs are likely to form unless forbidden by symmetry or spatial separation. The bond-like character of fractional CTCs should generally make them energetically favored over ion pairs. The latter may therefore often be metastable, and fractional CTC formation likely forms a universal degradation mechanism.[12]
4. Typically most doping-induced charge carriers are strongly bound in integer CTCs, with only a small portion of charge carriers contributing

to transport.[13, 14, 15, 16] The binding energy of these states in principle can be controlled by ionic size,[13, 17, 2] packing,[16] or disorder;[15, 18] however the small library of dopant molecules available limits optimization.

Because of these issues, many polymers still remain difficult or impossible to dope to useful carrier densities and/or conductivities, and material stability remains generally poor.

There is no *a priori* reason why the two steps in Figure 1a—charge-transfer and charge compensation—must be performed by the same chemical species. To illustrate this point, consider the other common doping method, electrochemical doping (Figure 1b). Here, an electrode performs the charge-transfer step, while the compensating ion originates from an electrolyte solution and is drawn into the film to maintain charge neutrality. Although the necessity of coating the film on a working electrode limits its applicability, electrochemical doping has one major advantage over molecular doping: the ion inserted into the film can be chosen from a huge library of commercially available salts. These ions are typically closed-shell species with wide electrochemical windows,[19] i.e. the ion reduction and oxidation potentials are typically separated from the redox potentials of the polymer (i.e. the oxidation potential for p-type polymers) by several volts. This property implies that charge-transfer from the ion back to the polymer is extremely unfavorable, and that ionization efficiency in electrochemically doped films are effectively 100%. For the same reason, significant hybridization cannot occur, thus fractional CTC formation is inhibited. These two factors suggest that using closed-shell electrochemically inert counter-ions should improve the stability of doped films. Just as critically, the wide range of ion sizes and shapes available also potentially allow for direct tuning of Coulombic trapping [13] and structural disorder effects when the ions are incorporated into the polymer.

Yamashita *et al.* recently proposed a hybrid ion-exchange doping method (Figure 1c)[20] that involves adding a concentrated electrolyte to a molecular doping solution. After the initial charge-transfer step, the dopant ion-exchanges with an electrolyte anion. If the exchange process is efficient, only the electrolyte counter-ion remains in the film, effectively giving a composition identical to that obtained by electrochemical doping. Thus, ion-exchange forms a bridge between molecular and electrochemical dop-

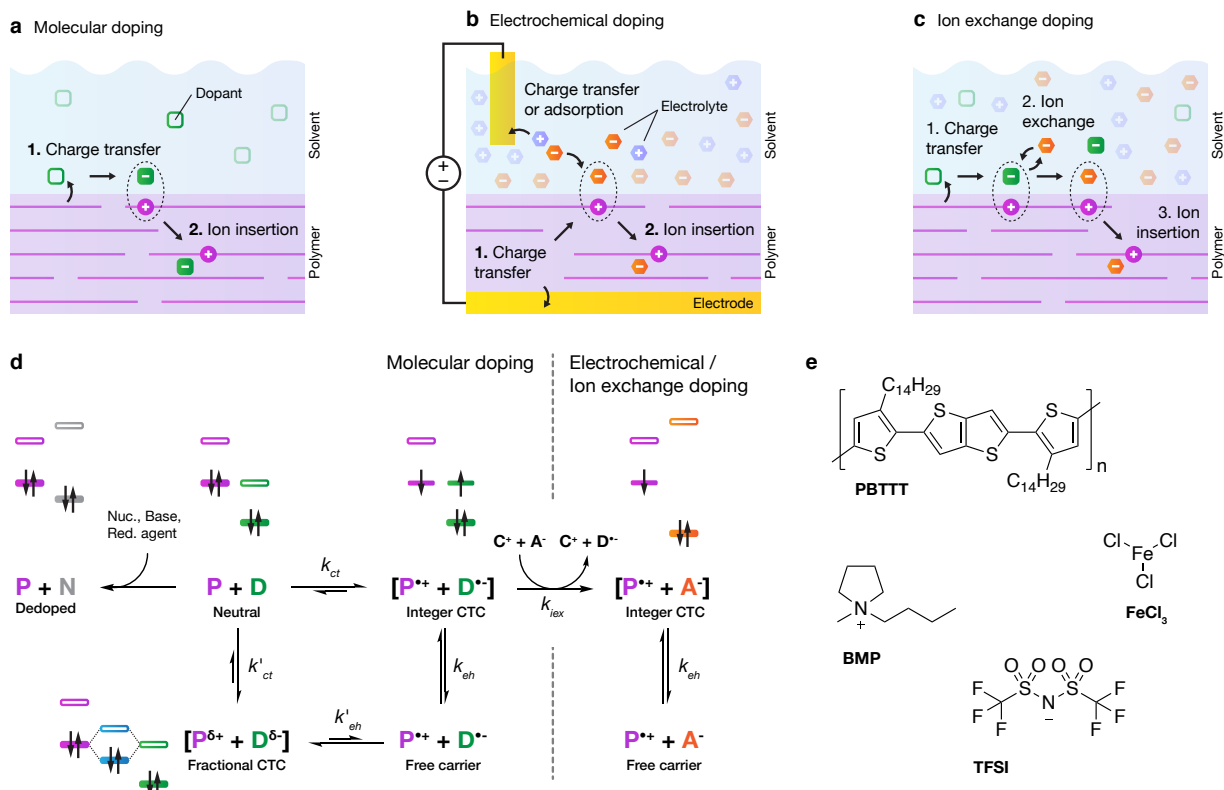


Figure 1: **Doping mechanism.** a) Molecular doping from an orthogonal solvent. b) Electrochemical doping. c) Ion-exchange doping. d) Reaction scheme for p-type molecular doping with ion-exchange. Representative electron configurations for each state is shown above/below; reorganization effects are neglected for clarity. e) Structures of the polymers studied in this work

ing, (k_{ex} equilibrium in Figure 1d) and combines the benefits of both techniques. Although ion-exchange has previously been applied to doped organic semiconductors,[21, 22, 23] the power of the technique was not demonstrated prior to the breakthrough by Yamashita *et al.* Their work convincingly demonstrated that ion-exchange can dramatically improve device stability and reach higher charge densities than typically achieved by molecular dopants.

The work of Yamashita in Ref. 20 provides a clear demonstration of the potential of ion exchange doping, but it also leaves open some key questions that need to be better understood to allow a full optimisation of the process and achieve higher electrical conductivities than what has been demonstrated with conventional charge transfer doping processes. One such question is the choice of the electrolyte solvent and the ionic liquid cation. Yamashita observed

a strong dependence of the achievable conductivity on the ionic liquid cation. This is puzzling as the cation should in principle not be involved in the process (Figure 1c). This limited understanding has so far prevented an optimisation of the process, and the highest conductivities reported in Ref. 20 for the PBTTT model system were only 600 S/cm, which are significantly below the highest conductivities reported in molecularly doped PBTTT[24, 25]. In the present work we aim to understand in more detail the key processes that govern ion exchange doping. In particular, we propose a framework that allows relating ion exchange doping to electrochemical doping for which a large body of literature exists already. The insight gained has allowed us to optimize the process and we report here for the first time high electrical conductivities in excess of 1000 S/cm in ion-exchanged samples of PBTTT.

Results

Theory of ion-exchange

Ion-exchange processes have been studied for well over a century, and the theoretical basis for ion-exchange is well understood.[26] Assuming both ions are monovalent, the exchange equilibrium can be described by the molar selectivity coefficient,

$$k_{ex} = \frac{C_{A,f}^- C_{D,s}^-}{C_{A,s}^- C_{D,f}^-} \quad (1)$$

where $C_{i,x}^z$ is the molar concentration of species i (dopant, D ; electrolyte anion, A), in phase x (solvent, s ; film, f), with charge indicated by superscript. We define the ion-exchange efficiency as the mole fraction of exchanged counter-ions divided by the total dopant density: $x_A = C_{A,f}^- / N^+$. Substituting this into Equation 1 and rearranging gives the following expression

$$x_A = 1 - x_D = \frac{k_{ex} C_{A,s}^-}{C_{D,s}^- + k_{ex} C_{A,s}^-} \quad (2)$$

This is the ion-exchange isotherm. It describes the efficiency of the ion-exchange process at equilibrium in terms of the concentration of each ion in solution and the selectivity coefficient. Interestingly, when $C_{D,s}^- = 1$, Equation 2 is equivalent to the Langmuir isotherm, which was previously found to describe the charge-transfer equilibrium, k_{ct} , in P3HT:F4TCNQ films.[27, 2, 28, 29] (Supporting Information Section 1).

We can see the impact of changing the electrolyte concentration more clearly using the identity $\Delta G_{ex}^0 = -kT \log(k_{ex})$ and separating the selectivity coefficient into two terms grouped by phase,

$$\ln \left(\frac{C_{A,f}^-}{C_{D,f}^-} \right) = \ln \left(\frac{C_{A,s}^-}{C_{D,s}^-} \right) - \frac{\Delta G_{ex}^0}{kT} \quad (3)$$

The first term of the right hand side of Equation 3 describes the concentration-dependent entropy contribution resulting from ion-exchange, while the second term describes the ionic selectivity of the polymer. When $|\Delta G_{ex}^0| \leq kT$, corresponding to $k_{ex} \sim 1$, the film does not show a strong preference for one ion versus the other. In this situation, the concentration of each ion can be controlled by varying the concentration ratio of electrolyte to dopant ions in solution. To achieve efficient ion-exchange, ΔG_{ex}^0 must be either negative, indicating the polymer prefers the

electrolyte ion, or weakly positive such that the selectivity can be overcome via the entropic term.

Exchange efficiency in PBTTT / FeCl₃ / BMP-TFSI

Our improved ion-exchange process follows a standard sequential solution doping process[27] using acetonitrile (AN) as the doping solvent, with the addition of a large excess of electrolyte. AN is an ideal solvent for ion-exchange doping for the same reasons as it is an ideal solvent for electrochemistry: it has an extremely wide electrochemical window (>6 V) and a high dielectric constant ($\epsilon_r = 38.8$), which allows us to use very high electrolyte concentrations.[30] As predicted by Equation 3 and shown experimentally below, high electrolyte concentrations are critical to achieving efficient ion-exchange. We use BMP TFSI as a model ion-exchange electrolyte because it is commercially available with low water content and very high purity. The TFSI ion itself also has several properties that make it well suited as a dopant ion—it is hydrophobic, has a wide electrochemical window, and is weakly interacting with most cations.[31]

Figure 2a shows UV-vis-NIR spectra of our model ion-exchange doping system, consisting of PBTTT thin films sequentially doped with a FeCl₃ / acetonitrile solution (1 mM) containing varying BMP TFSI electrolyte concentrations (1 μ M to 1 M). Molecular structures are given in Figure 2c. In all spectra, we observe complete bleaching of the polymer $\pi - \pi$ absorbance between 2 and 3 eV and the appearance of strong P1 and P2 polaron bands in the IR (<1 eV and 1.5 eV, respectively), consistent with a very high doping level. The two peaks visible in the UV at 3.2 and 3.9 eV are due to the presence of FeCl₄⁻ anions. A spectrum of FeCl₄⁻ in AN (dotted line, see Supporting Information Section 2 for details) is shown for comparison; the peaks are shifted slightly due to solvatochromism.

As the BMP TFSI electrolyte concentration is increased, we see a reduction in the FeCl₄⁻ absorption due to ion-exchange along with a conductivity increase of 20% (Figure 2b, blue squares), eventually reaching values in excess of 1000 S/cm. We can extract the residual FeCl₄⁻ concentration by fitting the UV portion of the absorption spectra (Supporting Information Section 3). From these fits, we obtain a carrier density of $5.8 \pm 0.5 \times 10^{20} \text{ cm}^{-3}$ for FeCl₃ doped films, corresponding to molar concentration of about 1 dopant per 1.5 PBTTT monomers. The increase

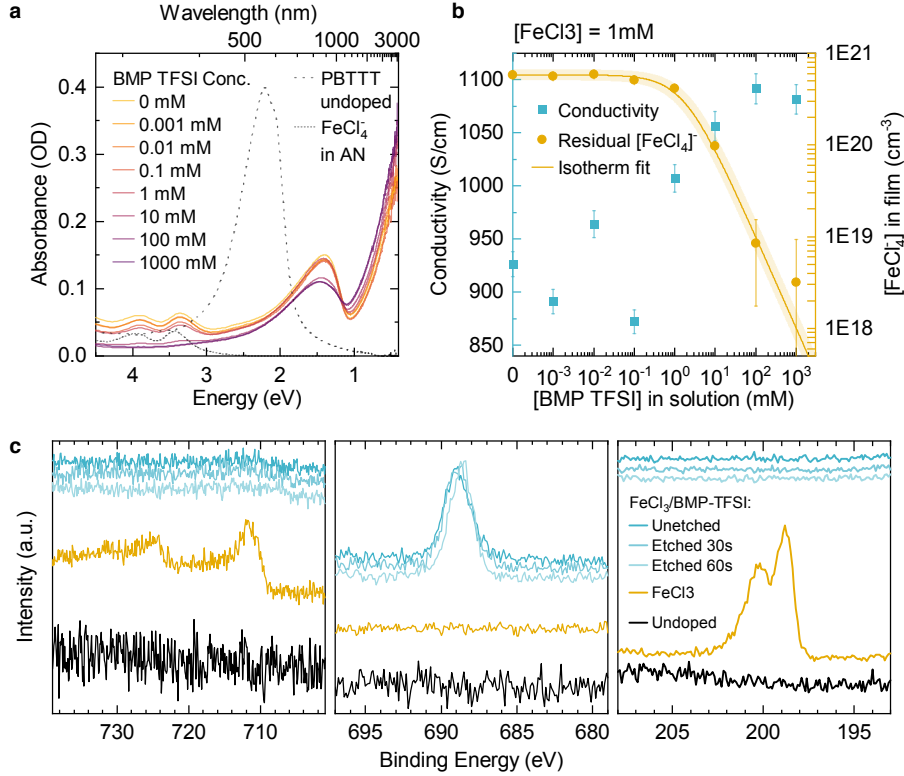


Figure 2: **Ion-exchange equilibrium.** a) UV-vis-NIR spectra of PBT TT films ion-exchange doped (100 sec.) with fixed 1 mM FeCl_3 concentration and varying BMP TFSI concentration. Undoped PBT TT (dashed line) and FeCl_4^- (dotted line) are shown for reference. b) Conductivity (blue squares) and residual FeCl_4^- concentration (yellow circles), obtained by fitting the absorption features from the films in (a). Solid line is a fit to the ion-exchange isotherm (Equation 2). c) Molecular structures of PBT TT, BMP TFSI, and FeCl_3 .

in P1 band intensity suggests carrier densities in ion-exchange doped films are higher still, although precise quantification of carrier density in PBT TT:TFSI is non-trivial. A quantitative analysis of the doping level in these films will be the focus of a separate work.

The yellow circles in Figure 2b show the residual FeCl_4^- concentration plotted vs. BMP-TFSI concentration in the doping solution, with FeCl_3 solution concentration fixed at 1 mM. Equation 2 allows us to fit these data (yellow line; shaded regions indicate 95% confidence interval). Using $C_{D,s}^- = 0.75$ mM (Supporting Information Section 2.2), we obtain $\Delta G_{ex}^0 = +29.3$ meV, indicating the polymer is weakly selective for FeCl_4^- . This value is roughly kT , therefore ion-exchange should be under entropic control when the electrolyte concentration is a few times higher than the FeCl_3 concentration.

Because the carrier density increases with increasing electrolyte concentration, using the FeCl_4^- concentrations we can only calculate a lower bound on the exchange efficiency. At a 100-fold molar excess of electrolyte the exchange efficiency is at least 98%, while at a 1000-fold excess it surpasses 99%, although both of these values may be limited by our fitting routine, which is not able to accurately determine FeCl_4^- concentrations below about 10^{19} cm⁻³. To further validate our optical measurements, we used XPS to determine the elemental Fe, Cl, and F compositions of PBT TT films before doping and after FeCl_3 (1 mM) or BMP-TFSI / FeCl_3 (100/1 mM) doping (Supporting Information Figure S5). These XPS data are fully consistent with our UV spectral fitting results, and confirm that FeCl_4^- to TFSI⁻ ion-exchange is highly efficient.

Importance of doping solvent choice

The high carrier density and exchange efficiency achieved here derive primarily from the choice of acetonitrile (AN) as the doping solvent, as opposed to n-butyl acetate used in previous works.[20, 32] These improvements stem from AN’s high dielectric constant, which increases electrolyte dissociation, and a dramatic increase in the reduction potential of Fe^{3+} ions in AN, which enables us to reach high carrier densities.

Figure 3a (yellow line) shows a spectrum of an anhydrous 1 mM FeCl_3 / acetonitrile (AN) solution identical to those used in the majority of our ion exchange doping experiments. This spectrum closely matches that of the FeCl_4^- anion[33, 34] indicating that in solution, a considerable fraction of FeCl_3 exists as FeCl_4^- . Since AN is aprotic and has an electrochemical window[35] extending well beyond the reduction potential of FeCl_3 [36] these anionic species cannot be the product of a redox reaction between FeCl_3 and the solvent. Instead, as described previously[37, 38] FeCl_3 disproportionates in anhydrous AN, resulting in an equilibrium between several ligand deficient cationic species and the anionic $[\text{FeCl}_4]^-$ complex; complete disproportionation corresponds to $4 \text{FeCl}_3 \longrightarrow \text{Fe}^{3+} + 3 [\text{FeCl}_4]^-$. Addition of excess chloride ions (Figure 3a, purple line) converts all iron in solution to FeCl_4^- . [38] The magnitude of the observed increase in FeCl_4^- absorption after the addition of excess chloride indicates that FeCl_3 almost completely dissociates to Fe^{3+} and FeCl_4^- in AN (see further discussion in Supporting Information Section 2.2).

Cyclic voltammetry measurements of FeCl_3 solutions in previous works have reported a rather low reduction potential, causing some confusion.[39] The observation that FeCl_3 dissociates to Fe^{3+} allows us to clear up these misconceptions. As a general rule, the reduction potential of iron(iii) should tend to increase as more chloride ligands are removed, because the Cl^- ions donate electron density to the metal center upon complexation.[40] From the reported $\text{Fe}^{3+} \rightleftharpoons \text{Fe}^{2+}$ redox potential in aqueous solution, 0.77 V vs. NHE,[41] we estimate a redox potential of about 0.15 V vs. Fc/Fc^+ , corresponding to about -5.2 eV vs vacuum, assuming the NHE absolute electrode potential is -4.44 eV.[42, 43] This would suggest that in aqueous solutions, FeCl_3 is similar in strength to F4TCNQ.

However, in anhydrous acetonitrile the $\text{Fe}^{3+} \rightleftharpoons \text{Fe}^{2+}$ redox couple was reported to be dramatically

stronger: a value of 1.57 V vs. AgNO_3 for 2 mM Fe^{3+} in anhydrous AN was reported by Kratochvil et al.[36] Assuming $\text{Fc}/\text{Fc}^+ = 0.1$ V vs. Ag/Ag^+ in AN[44] this corresponds to a redox potential of 1.47 V vs. Fc/Fc^+ , suggesting FeCl_3 in AN is significantly stronger than even CN6-CP, the strongest organic molecular dopant reported to date.[45] The reason for the strong solvent dependence of the FeCl_3 redox potential is complex, but likely derives from a combination of factors, including a larger crystal field splitting in AN vs water that stabilizes the Fe^{2+} state, and the intermediate dielectric constant of AN, which destabilizes the Fe^{3+} state relative to water, but is still high enough to permit strong dissociation of FeCl_3 . [36] The addition of small water impurities to FeCl_3 in AN was reported to lower the redox potential considerably, even in the presence of acid to prevent coordination by hydroxide ions.[36] This observation is consistent with our CV measurements of FeCl_3 solutions which showed $E_{1/2} = 0.8 \pm 0.08$ V, slightly higher than CN6-CP (Supporting Information Section 2). These findings indicate that water does not simply reduce the concentration of Fe^{3+} , for which the Nernst equation predicts a much weaker effect (59 mV/decade), but instead homogeneously decreases the redox strength of the solution without strongly affecting the concentration. To achieve high carrier densities, it is therefore critical that these solutions are prepared under dry conditions and used promptly, as AN is strongly hygroscopic.

The high dielectric constant of AN also enhances ion exchange efficiency. Previous implementations[20] of ion exchange doping used a relatively non-polar doping solvent, n-butyl acetate (nBA, $\epsilon_r = 5$). In low dielectric solvents, Coulomb interactions between electrolyte cations and anions are $\gg kT$, resulting in an effective free anion concentration that is considerably lower than the electrolyte concentration. In Yamashita et al, this effect manifested as an exchange efficiency that depended strongly on the electrolyte cation size.[20]

In a polar solvent such as AN ($\epsilon_r = 38$), the Coulomb interaction is dramatically weaker, and the electrolyte ions should be nearly fully dissociated at the high concentration used for ion exchange.[46] Under these conditions, the electrolyte cation is simply a spectator and plays no role in the doping process. Figure 3b shows UV-vis-NIR spectra of PBTFT films ion-exchange doped with several different cation:TFSI electrolytes (100:1 mM electrolyte: FeCl_3 , AN). We observe similarly high

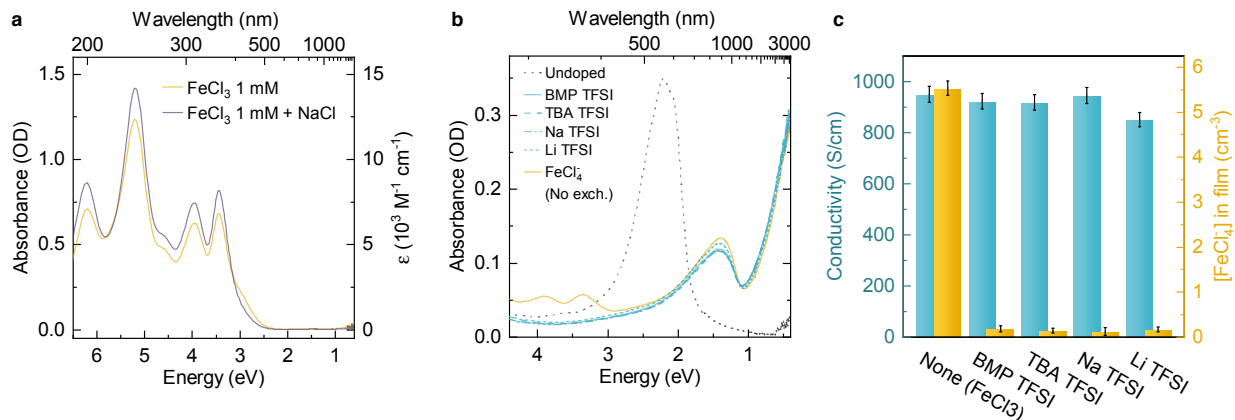


Figure 3: **Details of ion exchange doping mechanism in acetonitrile** a) UV-vis-NIR spectra of a FeCl_3 (1 mM in AN, anhydrous), and the same solution with excess NaCl added. Spectra were taken in 1 mm path length quartz cuvettes sealed under N_2 ; AN and cuvette background have been subtracted. Right axis shows the calculated molar absorptivity (ϵ). b) UV-vis-NIR spectra of PBTTT films doped with varying electrolytes (100/1 mM electrolyte/ FeCl_3 , AN, 300 s). Spectra of undoped PBTTT and PBTTT: FeCl_4^- (1 mM FeCl_3 , AN, 300 s) shown for reference. c) Conductivity (blue, left axis) and extracted FeCl_4^- concentration (yellow, right axis) for films shown in (b).

ion-exchange efficiency to within error with all cations (Figure 3c), in contrast with the results of Yamashita *et al.*[20] A very slightly lower doping level and electrical conductivity (Figure 3c) is observed in Li TFSI presumably due to its higher water content (specified as 1%) which reduces the redox potential of Fe^{3+} , as discussed previously. However for all cations, the conductivities obtained here are significantly greater than the value of about 600 S/cm obtained in Ref. 20.

Kinetics of ion exchange doping

In the theory of ion exchange given in the preceding sections, we assume the system is at equilibrium. Therefore, it is critical to understand the kinetics of both the charge transfer and ion exchange processes to ensure our measurements are performed on samples which have fully equilibrated. Figure 4 shows UV-vis-NIR and FTIR spectroscopy, along with conductivity and GIWAXS data for PBTTT films ion exchange doped for varying times using our standard ion exchange process (100/1 mM BMP TFSI / FeCl_3 , AN).

UV-vis-NIR spectra (Figure 4a) show a continuous bleaching of the polymer $\pi - \pi^*$ band, with nearly complete bleaching at 10 seconds and further slow bleaching continuing up to 60 seconds. The P1 band

(<1 eV) increases continuously over the entire time period, while the P2 band (1.5 eV) peaks at 6 seconds and then slowly decreases with extended doping times. The decrease in P2 at high doping levels is consistent with previous reports in OECT devices at high doping levels in PBTTT, where this decrease was assigned to bipolaron formation.[47] However, the bipolaron band is generally understood to appear at a wavelength intermediate between P1 and P2,[48] while no such band is observed here.

The FTIR spectra (Figure 4b) likewise show no evidence of bipolaron formation. At short doping times (≤ 3 s) the P1 band is centered at higher energy (~ 0.3 eV) with a weak shoulder below 0.2 eV; these two features correspond to intra-chain and inter-chain transitions, respectively.[49] At longer doping times, above 10 seconds, we observe a red shift in the P1 band, which is eventually dominated by the low energy, inter-chain feature at long doping times (i.e. high carrier densities). The continuous redshift and increase in P1 band intensity is consistent with increasing polaron delocalization at high carrier density; we observe no signatures which can be attributed to bipolarons. It is plausible that the reduction in P2 band intensity could presumably arise from a weakening of the oscillator strength of this transition due to changes in polymer structure or doping level; similar

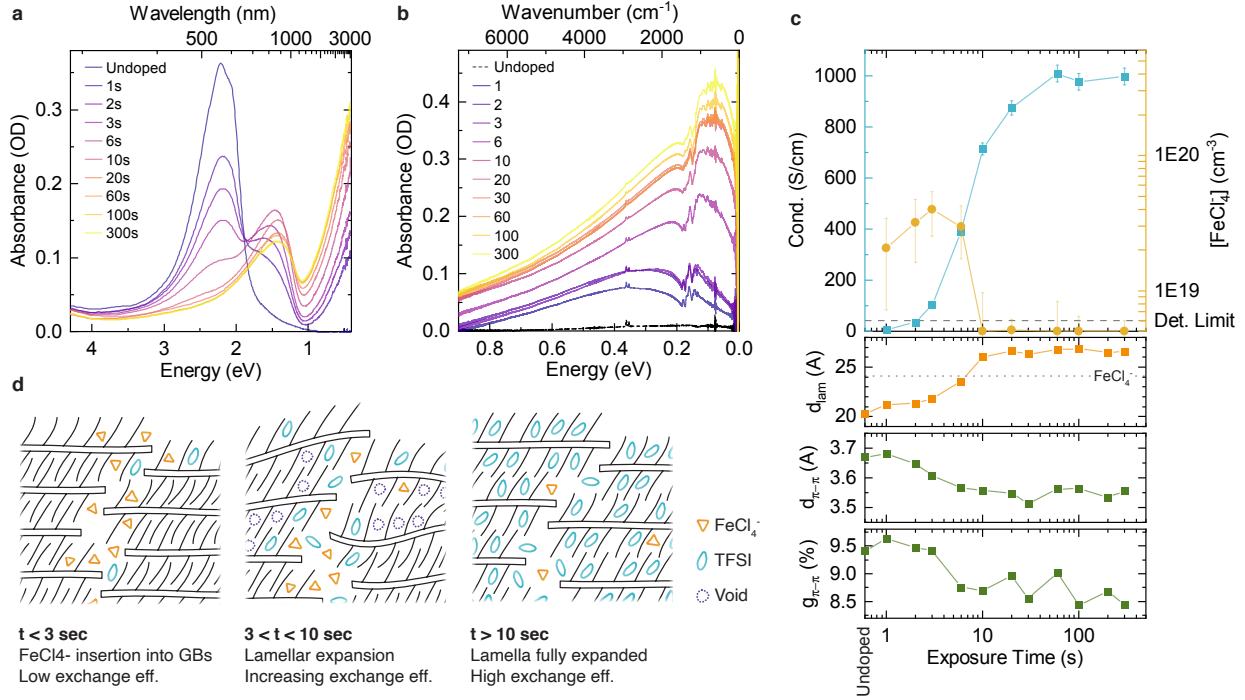


Figure 4: **Kinetics of ion exchange doping** Doping solutions consisted of 100 /1 mM BMP TFSI / FeCl_3 in AN. a) UV-vis-NIR spectra. b) FTIR spectra. c) Electrical conductivity, residual FeCl_4^- (extracted from UV-vis spectra), unit cell parameters and $\pi - \pi$ paracrystallinity (extracted from GIWAXS data) as a function of doping time. d) Illustration of film microstructure at different doping times.

effects were recently described by Spano and coworkers for the P1 band.[49]. However a more detailed theoretical interpretation of these results will be required.

In both sets of spectroscopic data, there is clear change in behavior occurring at about 6 seconds—the P2 intensity reaches a maximum at 6 seconds, while the P1 intensity increases dramatically and strongly redshifts. This is correlated with transitions observed in the conductivity, FeCl_4^- concentration, and GIWAXS structural data (Figure 4c). At short doping times, below 3 seconds, the lamellar stacking distance remains about 21 Å nearly the same as undoped PBTTT (20.2 Å) and much smaller than observed in highly doped PBTTT:TFSI (26.5 Å) or PBTTT: FeCl_4^- (24.1 Å). This short stacking distance, along with the sizable charge carrier density visible in the UV-vis spectrum, implies preferential doping of grain boundaries or crystalline defect sites. The FeCl_4^- concentration reaches a peak at 3 seconds, indicating that in this regime the exchange efficiency

is quite low and that FeCl_4^- ions penetrate the film more quickly, presumably due to their smaller size.

However, above 6 seconds the concentration of FeCl_4^- in the film drops dramatically, indicating that the rate of TFSI ion insertion becomes much faster than FeCl_4^- . The persistently low FeCl_4^- concentration in this regime, even as the doping level continues to increase, implies two things. First, ion exchange has clearly become much more efficient than at earlier times, and thus the equilibrium ΔG_{ex} obtained previously appears to be more positive at early stages of the doping process. Second, the sharp drop in FeCl_4^- concentration implies that the ion exchange equilibrium is established more quickly than the redox process, and therefore that the overall doping rate is limited by the redox step.

The observed change in behavior at 6 seconds appears to be driven by a sudden expansion in the lamellar stacking distance, which increases from about 21 to 26.5 Å between 3 and 10 seconds (Figure 4c). The rapidity of this change is suggestive of a

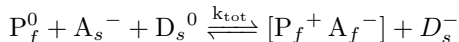
structural phase transition in which the intercalation of ions into the lamella generates voids in neighboring sites, greatly increasing the rate of ion intercalation. An illustration of this mechanism is shown in Figure 4d. Similar behavior in an OECT device was recently observed by Bischak *et al.*[50] This nucleated ion-intercalation behavior can be understood as resulting from an interaction between the energetic cost of distorting the polymer crystal to incorporate an ion and the polymer redox potential. After an initial ion intercalates, the redox potential of adjacent sites decreases, because the lamella nearby are already partially “unzipped.” We can see further evidence for this phase transition in the broadening of the lamellar stacking peaks observed in the 6 second GIWAXS linecuts (Supporting Information Figure S12), consistent with heterogeneous FeCl_4^- and TFSI dominated domains. The polymer π -stacking behavior also shows a sharp drop in paracrystallinity at 6 seconds doping time, consistent with a sudden increase in doping within crystalline domains. This effect is due to backbone planarization driven by polaron delocalization, visible as the redshift of the FTIR spectra discussed previously.

Reducing the doping solution concentration while maintaining a fixed BMP TFSI / FeCl_3 ratio and 100 s doping time (Supporting Information Section 5) likewise shows a drop in exchange efficiency. This further indicates that the observed low exchange efficiency prior to lamellar expansion is due to an increase in ΔG_{ex} , rather than slow ion exchange kinetics. In contrast, the ion exchange kinetics of P3HT (Supporting Information Section 6), which is understood to have disordered side chains in contrast with the highly interdigitated side chains of PBTTT,[51] shows no evidence of a phase transition, reinforcing our understanding of the connection between crystalline order and ΔG_{ex} .

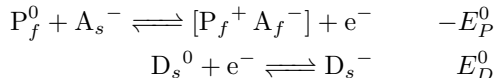
Together, these results give a clear insight into the microscopic mechanism of ion exchange doping in PBTTT revealing a clear doping level dependence of exchange efficiency. These findings suggest that in the ideal regime where electrolyte association does not limit the ion exchange efficiency, ΔG_{ex}^0 is primarily controlled by the energetics of distorting the polymer crystal to incorporate the ion.

Comparison with electrochemical doping

When the electrolyte concentration is sufficiently high that the electrolyte ion insertion dominates (i.e., the ion-exchange efficiency is high), the overall ion-exchange reaction is simply an ion insertion reaction coupled with a redox reaction between the oxidizing agent and polymer,



For clarity, we can decompose this reaction into two half-cell reactions,



The first reaction corresponds exactly to electrochemical doping with an applied potential E_P^0 , while the second reaction is the solution-state reduction potential E_D^0 of the dopant molecule measured by e.g. cyclic voltammetry (CV). At equilibrium, $E_D^0 - E_P^0 = 0$; therefore, the doping level generated by ion-exchange corresponds precisely to that prepared by electrochemical doping equilibrium with an applied voltage equal to the reduction potential of the dopant. For further discussion, see Supporting Information Section 1.3. In this sense, we expect that any strong oxidizing agent should be capable of doping polymer films, and that the achievable carrier density and conductivity should depend only on the oxidizer’s reduction potential, so long as the exchange efficiency remains high.

Here, we compare 12 different dopants with reduction potentials from -0.25 to 1 V vs. Fc/Fc^+ , shown in Figure 5a. UV-vis-NIR spectra (Supporting Information Figure S10) indicate that ion-exchange efficiency remains high across all the oxidizing agents studied here. Figure 5c shows the electrical conductivity of the films in 5b plotted against the reduction potential of each dopant (see CV measurements in Supporting Information Section 2.1). For comparison, we also show the conductivity of a PBTTT electrochemical transistor gated using the same electrolyte (100 mM BMP TFSI) used for ion-exchange. We observe good qualitative agreement between the electrochemical device and our ion-exchange data, consistent with our analysis above.

Electrodes typically behave as completely innocent oxidizing agents, meaning that they participate in outer-shell electron-transfer reactions only.[52] How-

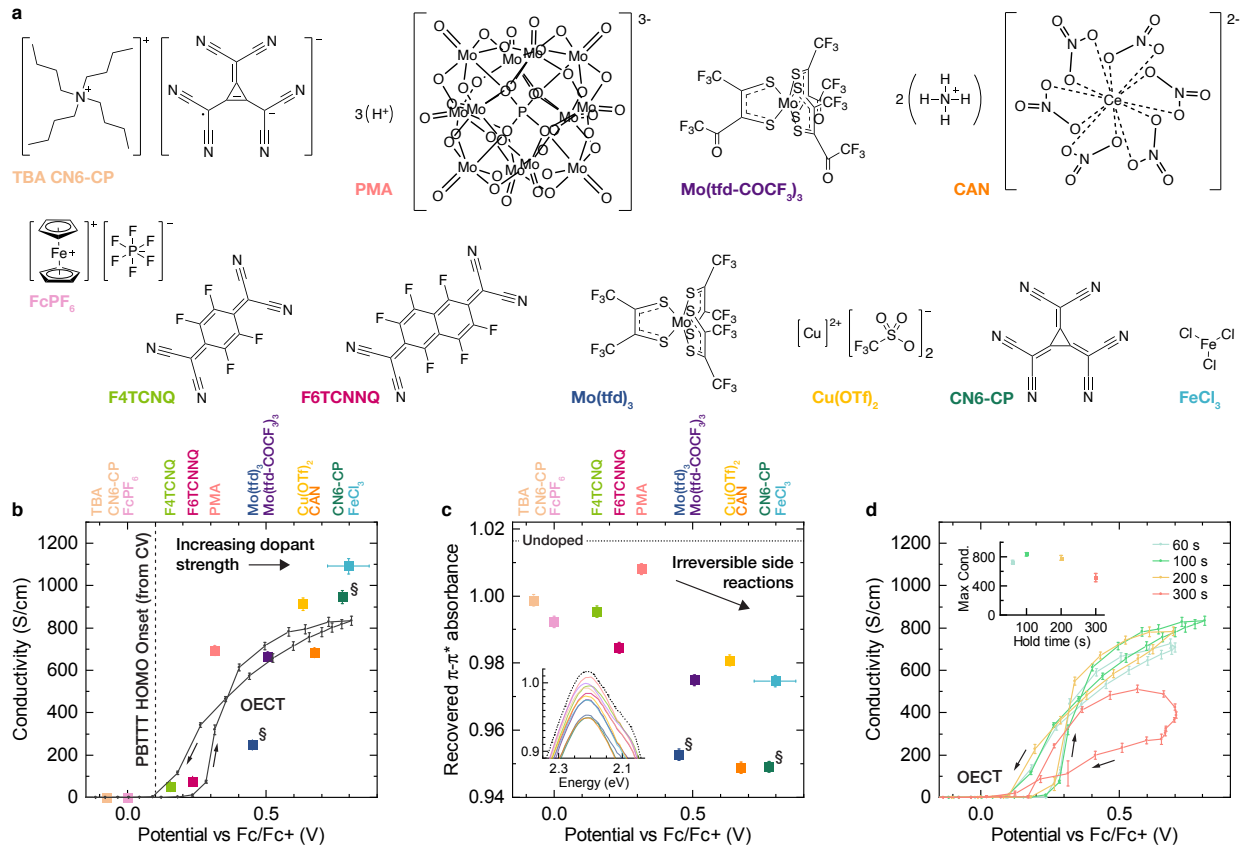


Figure 5: **Characterizing dopant strength.** a) Chemical structures of dopants used in this study. b) Plot of conductivity vs. dopant reduction potential (vs Fc/Fc+), for ion-exchange doped PBTTT films and a PBTTT OECT. Both ion-exchange and OECT devices use a 100 mM BMP-TFSI / AN electrolyte. Dopant concentration and exposure time was 1 mM and 100 sec, respectively. Vertical dashed line shows the oxidation onset for PBTTT (corresponding to the HOMO level edge) measured by CV. c) Recovered $\pi - \pi^*$ absorbance after chemically dedoping films in (b), normalized by each film's as cast $\pi - \pi^*$ absorbance; inset shows the normalized dedoped spectra. The dotted line labelled "undoped" indicates the increase in $\pi - \pi^*$ band intensity observed when an undoped film is treated with the same dedoping solution; this increase is due to removal of doping impurities.[4] § indicates the dopant displayed limited solubility in AN (<1 mM). d) Conductivity vs. redox potential for OECT devices gated for varying gate hold times at each data point; inset shows the maximum conductivity reached as a function of hold time.

ever, chemical redox agents, products of chemical redox reactions, or the electrolyte itself may participate in other types of reactions with the polymer, such as proton transfer, substitution or elimination reactions. In general, we would expect these types of reactions to degrade the functional properties of the polymer by introducing disorder. In this sense, the quantitative mismatch between the OECT and ion-exchange data suggests that conductivity is limited by both chemical degradation by dopants and by

intrinsic polymer instability.

To quantify such non-innocent behavior, we collected UV-vis spectra of each sample before doping and after dedoping with a diethylamine/acetone solution, which was previously shown to quantitatively dedope P3HT:F4TCNQ films.[4] Assuming the films are initially undoped and the oxidizing agent is completely innocent, the $\pi - \pi^*$ band intensity after dedoping should recover to the same value as measured before doping. A decrease in recovered $\pi - \pi^*$ ab-

sorbance therefore is a signature of irreversible side reactions.

Figure 5d shows the recovered $\pi-\pi^*$ absorbance for each sample. Within a given oxidizing strength range, there is a strong correlation between higher conductivity and higher $\pi-\pi^*$ recovery, for instance comparing Mo(tfd-COCF₃)₃ and Mo(tfd)₃, Cu(OTf)₂ and CAN, or CN6-CP and FeCl₃, indicative of varying degrees of non-innocent oxidation reactions. Furthermore, we observe a clear reduction in $\pi-\pi^*$ band recovery with increasing oxidizing agent strength, suggestive of an intrinsic polymer instability at high redox potentials.

We see direct evidence for this intrinsic polymer degradation in the OECT data (Figure 5d). During the OECT measurement, the device must be held at each gate voltage for a period before measurement to allow for formation of the electrochemical double layer and diffusion of electrolyte anions into the bulk of the polymer film. In the absence of degradation reactions, we would expect to see a monotonic increase in conductivity with increasing gate hold time. However, our measurements show that conductivity reaches a peak at 100 seconds hold time (Figure 5d, inset) with a strong decline in conductivity and increase in hysteresis at longer hold times. This reactivity must originate from the polymer itself, as the electrolyte itself is stable against reduction potentials exceeding 2 volts vs. Fc/Fc⁺. Because this degradation is cumulative—i.e. the conductivity at high potentials is limited by the degradation built up during the scan through lower potentials—the conductivity in our OECT devices is lower than achievable via ion-exchange.

At very high doping levels there is therefore a trade-off between the time required to inject the compensating ions and the timescale of degradation reactions. In our optimized ion-exchange process using FeCl₃, device conductivity is stable for doping times from 60 to 300 seconds (Figure 4c). Therefore, degradation seems to be relatively slow on the timescale required to reach doping equilibrium, although the plateau in conductivity could still result from a competition between further carrier density increases and a reduction in mobility due to degradation.

Our measurements of doped film stability in nitrogen, air, and under thermal stress (Supporting Information Section XX) echo the above findings. Although ion exchange does improve the stability of doped films, we observe significant degradation even at temperatures well below those at which TFSI-

based ionic liquids typically decompose. The intrinsic instability of highly doped PBTTT observed here is consistent with our observation of only moderate improvement in environmental stability. Our findings indicate that ion exchange provides a clear path forward in engineering highly doped and stable polymer films, but that the identification of intrinsic polymer degradation mechanisms under electrochemical stress, or in the presence of environmental impurities like water, are critical next steps in engineering highly conductive and stable polymer films.

Conclusions

We have demonstrated that ion-exchange doping with FeCl₃ can generate highly ordered polymer films with extremely high doping levels. We find that the process is most efficient in highly polar solvents with large electrochemical window, such as acetonitrile, in which the ionic liquid cation is a mere spectator ion, and that the ion exchange efficiency can be controlled entropically simply by adjusting the electrolyte concentration, even in situations where the free energy for ion exchange is weakly positive. We have also shown that the ion exchange process can essentially be understood as analogous to electrochemical doping wherein the redox potential of the dopant plays the role of the applied electrical voltage. This improved understanding reported in our work has allowed the optimization of the achievable electrical conductivity of ion-exchange doped PBTTT films, for which we have reported conductivities in excess of 1000 S/cm. It also paves the way for fundamental studies of charge transport in ion-exchange doped conjugated polymers, which make use of the broad choice of the size and shape of the ionic liquid anions that are now available to tune the electrostatic interactions between the mobile polarons on the polymer and the counterions. Ion exchange doping is an important approach that is likely to become widely used to control the electrical properties of conjugated polymers.

Methods

Materials

PBTTT (poly(2,5-bis(3-alkylthiophen-2-yl)thieno(3,2-b)thiophene); Mw = XX kDa, PDI = XX) was synthesized as described previously.[53] P3HT (poly(3-hexylthiophene-2,5-diyl); 99.0% RR,

Mw = 44 kDa, PDI 2.1) was purchased from TCI. Ion-exchange salts Li-TFSI (>99%, <1% water), Na-TFSI (>97%), BMP-TFSI (>98.5%, <0.04% water), and TBA-TFSI (>99%) were purchased from Sigma Aldrich. Dopants PMA (hydrated, ACS reagent), Fc-PF₆ (>97%), Cu(OTf)₂ (>98%), FeCl₃ (anhydrous, >99.99% trace metals basis), OA, and CAN (>99.99% trace metals basis) were purchased from Sigma Aldrich. F4TCNQ (>98%) was obtained from TCI. TBA CN6-CP, F6TCNNQ, Mo(tfd)₃, Mo(tfd-COCF₃)₃, and CN6-CP were synthesized as described previously[54, 55, 56, 57, 58, 45]. Anhydrous acetonitrile (Romil Hi-Dry, <20 ppm water) was used to prepare all doping solutions, while anhydrous dichlorobenzene and chlorobenzene (Romil Hi-Dry, <20 ppm water) were used for polymer solution preparation; further details are given below. Acetone and diethylamine for dedoping experiments were obtained from Romil and Sigma Aldrich, respectively. All materials were used as received.

Solution Preparation

Solutions of PBTTT were prepared in 1,2-dichlorobenzene (DCB) at a concentration of 10 mg/mL and heated at 80° C overnight before use. Stock electrolyte solutions (1M in AN) were prepared before use and stored in the glovebox until needed; dopant solutions (10 mM) were prepared immediately before use. All polymer and doping solution preparation, including weighing reagents, was performed in an inert atmosphere (<1 ppm H₂O, O₂ during solution preparation; <10 ppm H₂O, O₂ during weighing).

Sample Preparation

Glass substrates (Corning Eagle XG) for conductivity and UV-vis measurements were cut into 1 cm squares, and 1 mm electrical contacts (Cr/Au, 5/25 nm) were deposited in each corner via thermal evaporation through a shadow mask. OECT and Hall bar samples were prepared on the same substrates using double-layer liftoff photolithography. Hall bar samples used contact thicknesses identical to conductivity samples; OECT devices used thicker contacts (Cr/Au, 5/200 nm) to ensure a small series resistance (see OECT details below). Samples for GI-WAXS measurement were prepared on Si (native oxide) and cleaned using the same procedure. FTIR

samples were coated onto double side polished undoped Si, also cleaned using the above procedure. Substrates were cleaned by sequential sonication in 2% Decon 90/DI water, DI water, acetone, and isopropanol, then dried with nitrogen flow and exposed to oxygen plasma (300 watts, 10 minutes) before use.

PBTTT films were spin coated from 80° C solutions using preheated glass pipettes onto 80° C substrates. Samples were spun at 1500 rpm until dry (60 seconds) and subsequently annealed in N₂ at 180° C for 20 minutes, then slowly cooled to room temperature by switching off the hotplate.

Ion-exchange doping solutions were prepared immediately before use due to the limited stability of many dopants in the presence of dilute water impurities. To obtain a standard 100:1 mM electrolyte:dopant concentration, electrolyte stock solutions (1 M) and oxidizer stock solutions (10 mM) were mixed with acetonitrile at 1:1:8 ratio, respectively. Samples were sequentially doped with 150 uL doping solution per cm² substrate area, waiting a variable delay period, then spinning off the excess solution at 8000 rpm. While spinning, samples were washed with 1 mL acetonitrile to remove excess electrolyte and dopant from the surface.

Conductivity Measurements

Conductivity was measured in van der Pauw configuration.[59, 60] Measurements were performed using an Agilent 4155B sourcemeter under nitrogen atmosphere (<20ppm O₂). Four measurements were performed per sample by measuring a 2-point I-V hysteresis sweep (-0.1 to 0.1 V) between each pair of adjacent electrodes, while simultaneously monitoring the voltage at the remaining two electrodes. The resulting 4 point resistance data was checked for hysteresis, current reversal, and reciprocity ($\frac{V_{12}}{V_{34}} = \frac{V_{34}}{V_{12}}$) to a tolerance of 3%, in line with NIST recommendations.[61] Uncertainties are dominated by thickness uncertainty; contact size effects contribute <1% to the relative error.[59, 60] Thickness measurements were performed using a Bruker Dektak XT. Conductivity values are calculated using the undoped film thickness to prevent thickness variations from creating apparent differences in charge transport properties between samples.

OECT Measurements

OECT devices were measured in a two point geometry. After spin coating the polymer onto substrates

with pre-patterned electrodes, the polymer layer was removed to define the device active area. Device length was 4000 μm ; widths varied between devices and were measured via surface profilometry after measurement (650 to 1200 μm , std. dev. <50 μm within each device). Thick electrodes (5/200 nm Ti/Au) were used to reduce the total series resistance to 65 ohms; the minimum device resistance measured was 1600 ohms.

PDMS spacers (3 mm thick) were prepared with Sylgard 184 10:1 w/w base to crosslinker ratio and baked at 60C for 1.5 hours in an oven. The spacers were patterned to expose the active area, then immersed in acetonitrile overnight to remove any residual crosslinker. To form the OECT, a silver quasi-reference electrode identical to those used in our CV measurements (Ag oxidized by O_2 plasma 300 W, 1 min) was pierced through the side of a spacer, then placed on top of the device substrate and filled with electrolyte (100 mM BMP TFSI in AN) under nitrogen atmosphere (<1 ppm H_2O , O_2). The electrolyte well was sealed with a Pt sheet acting as the gate electrode, and clamped together between two acrylic sheets. The resulting assembly remained airtight for over 24 hours.

After sealing the device, measurements were performed in air using an Agilent 4155B sourcemeter. Source drain I-V measurements used a voltage range from -0.1 to 0.1 V. Gate voltage was swept from 0 to 1.3 V and back in 0.1 V increments. Before the I-V measurement at each gate voltage, the device was held with the gate on and 0 V source-drain voltage for a hold time (varying between 60 and 300 seconds; see Figure 5d). The hold time was fixed for each gate voltage sweep; new devices were used for each different hold time measurement. The potential of the silver reference was measured during each I-V measurement, which was converted to V vs. Fc/Fc^+ using a separate CV measurement.

Spectroscopy

UV-vis-NIR spectra were collected on a Shimadzu UV-3600i dual beam spectrometer, using a 3 nm slit width and 2 nm data interval. Substrate background spectra were collected separately. IR (<0.75 eV) and UV (>3.02 eV) regions were smoothed using a Savitzky-Golay filter;[62] the filter window was 50 points in the IR and 10 points in the UV. FTIR spectra (SI) were collected on a Bruker Vertex 70V using a DLATGS detector.

GIWAXS Characterization

Grazing-incidence Wide-angle X-ray Scattering (GIWAXS) measurements were performed at Beamline 8-ID-E at the Advanced Photon Source (APS) at Argonne National Laboratory. Samples were irradiated with a 10.9 keV X-ray at an incidence angle 0.13° for 2 summed exposures of 2.5 second (5 s of exposure in total), and scattered X-rays were recorded by a Pilatus 1 M detector located 228.16 mm from the sample. The collected images were then processed by using the GIXSGUI software.[63] The background was subtracted by fitting the curves to an exponential decay, and peaks were fitted to Gaussian functions. Peak widths and positions were used to calculate the $\pi-\pi$ paracrystallinity assuming the coherence length is dominated by paracrystalline disorder, as previously suggested by Rivnay et al:[64]

$$g = \frac{1}{2\pi} \sqrt{\Delta_q d_{hkl}} \quad (4)$$

where Δ_q is the diffraction peak full width at half maximum, and d_{hkl} is the interplanar distance.

Acknowledgements

I.E.J acknowledges funding through a Royal Society Newton International Fellowship. Financial support from the European Research Council for a Synergy grant SC2 (no. 610115) and from the Engineering and Physical Sciences Research Council (EP/R031894/1) is gratefully acknowledged. Y.L. thanks the European Commission for a Marie-Sklodowska-Curie fellowship. For PhD fellowships D.S. thanks the EPSRC CDT in Sensor Technologies for a Healthy and Sustainable Future (Grant No. EP/L015889/1), L.L. the EPSRC CDT in graphene technology and D.T. the Cambridge Commonwealth European and International Trust. S.B. and S.R.M. thank National Science Foundation (through the DMREF program, DMR-1729737). This research used resources of the Advanced Photon Source, a U.S. Department of Energy (DOE) Office of Science User Facility, operated for the DOE Office of Science by Argonne National Laboratory under Contract No. DE-AC02-06CH11357. We thank Yadong Zhang for some dopant synthesis, and Mohamed Al-Hada for assistance with XPS measurements.

References

- [1] Ingo Salzmann, Georg Heimel, Martin Oehzelt, Stefanie Winkler, and Norbert Koch. Molecular electrical doping of organic semiconductors: Fundamental mechanisms and emerging dopant design rules. *Accounts of Chemical Research*, 49(3):370–378, 03 2016.
- [2] Ian E. Jacobs and Adam J. Moulé. Controlling molecular doping in organic semiconductors. *Advanced Materials*, page 1703063, 2017.
- [3] Björn Lüssem, Chang-Min Keum, Daniel Kasemann, Ben Naab, Zhenan Bao, and Karl Leo. Doped organic transistors. *Chemical Reviews*, 116:13714–13751, 2016.
- [4] Ian E. Jacobs, Faustine Wang, Nema Hafezi, Cristina Medina-Plaza, Thomas F. Harrelson, Jun Li, Matthew P. Augustine, Mark Mascall, and Adam J. Moulé. Quantitative dedoping of conductive polymers. *Chemistry of Materials*, 29(2):832–841, 01 2017.
- [5] Jack Fuzell, Ian E. Jacobs, Sophia Ackling, Thomas F. Harrelson, David M. Huang, Delmar Larsen, and Adam J. Moulé. Optical dedoping mechanism for p3ht:f4tcnq mixtures. *The Journal of Physical Chemistry Letters*, pages 4297–4303, 10 2016.
- [6] Jing Li, Ivan Duchemin, Otello Maria Roscioni, Pascal Friederich, Marie Anderson, Enrico Da Como, Gabriele Kociok-Köhn, Wolfgang Wenzel, Claudio Zannoni, David Beljonne, Xavier Blase, and Gabriele D’Avino. Host dependence of the electron affinity of molecular dopants. *Materials Horizons*, 6(1):107–114, 2019.
- [7] Ingo Salzmann, Georg Heimel, Steffen Duhm, Martin Oehzelt, Patrick Pingel, Benjamin M. George, Alexander Schnegg, Klaus Lips, Ralf-Peter Blum, Antje Vollmer, and Norbert Koch. Intermolecular hybridization governs molecular electrical doping. *Physical Review Letters*, 108(3):035502, 01 2012.
- [8] Amer Hamidi-Sakr, Laure Biniek, Jean-Louis Bantignies, David Maurin, Laurent Herrmann, Nicolas Leclerc, Patrick Lévêque, Vishnu Vijayakumar, Nicolas Zimmermann, and Martin Brinkmann. A versatile method to fabricate highly in-plane aligned conducting polymer films with anisotropic charge transport and thermoelectric properties: The key role of alkyl side chain layers on the doping mechanism. *Advanced Functional Materials*, 27(25):1700173–n/a, 2017.
- [9] Keehoon Kang, Shun Watanabe, Katharina Broch, Alessandro Sepe, Adam Brown, Iyad Nasrallah, Mark Nikolka, Zhuping Fei, Martin Heeney, and Daisuke Matsumoto. 2d coherent charge transport in highly ordered conducting polymers doped by solid state diffusion. *Nature materials*, 15(8):896–902, 2016.
- [10] D Tyler Scholes, Patrick Y Yee, Jeffrey R Lindemuth, Hyeyeon Kang, Jonathan Onorato, Raja Ghosh, Christine K Luscombe, Frank C Spano, Sarah H Tolbert, and Benjamin J Schwartz. The effects of crystallinity on charge transport and the structure of sequentially processed f4tcnq-doped conjugated polymer films. *Advanced Functional Materials*, 2017.
- [11] Ian E. Jacobs, Camila Cendra, Thomas F. Harrelson, Zaira I. Bedolla Valdez, Roland Faller, Alberto Salleo, and Adam J. Moulé. Polymorphism controls the degree of charge transfer in a molecularly doped semiconducting polymer. *Materials Horizons*, 5(4):655–660, 2018.
- [12] Kristen E. Watts, Bharati Neelamraju, Erin L. Ratcliff, and Jeanne E. Pemberton. Stability of charge transfer states in f4tcnq-doped p3ht. *Chemistry of Materials*, 31(17):6986–6994, 09 2019.
- [13] V. I. Arkhipov, E. V. Emelianova, P. Heremans, and H. Bässler. Analytic model of carrier mobility in doped disordered organic semiconductors. *Physical Review B*, 72(23):235202–, 12 2005.
- [14] P. Pingel and D. Neher. Comprehensive picture of p-type doping of p3ht with the molecular acceptor f4tcnq. *Physical Review B*, 87:115209, Mar 2013.
- [15] Max L. Tietze, Johannes Benduhn, Paul Pahner, Bernhard Nell, Martin Schwarze, Hans Kleemann, Markus Krammer, Karin Zojer, Koen Vandewal, and Karl Leo. Elementary steps in electrical doping of organic semiconductors. *Nature Communications*, 9(1):1182, 2018.

- [16] Martin Schwarze, Christopher Gaul, Reinhard Scholz, Fabio Bussolotti, Andreas Hofacker, Karl Sebastian Schellhammer, Bernhard Nell, Benjamin D. Naab, Zhenan Bao, Donato Spoltore, Koen Vandewal, Johannes Widmer, Satoshi Kera, Nobuo Ueno, Frank Ortmann, and Karl Leo. Molecular parameters responsible for thermally activated transport in doped organic semiconductors. *Nature Materials*, 18(3):242–248, 2019.
- [17] Taylor J. Aubry, Jonathan C. Axtell, Victoria M. Basile, K. J. Winchell, Jeffrey R. Lindemuth, Tyler M. Porter, Ji-Yuan Liu, Anastassia N. Alexandrova, Clifford P. Kubiak, Sarah H. Tolbert, Alexander M. Spokoyny, and Benjamin J. Schwartz. Dodecaborane-based dopants designed to shield anion electrostatics lead to increased carrier mobility in a doped conjugated polymer. *Advanced Materials*, 31(11):1805647, 2020/06/02 2019.
- [18] Artem Fediai, Franz Symalla, Pascal Friederich, and Wolfgang Wenzel. Disorder compensation controls doping efficiency in organic semiconductors. *Nature Communications*, 10(1):4547, 2019.
- [19] Michel Armand, Frank Endres, Douglas R. MacFarlane, Hiroyuki Ohno, and Bruno Scrosati. Ionic-liquid materials for the electrochemical challenges of the future. *Nature Materials*, 8(8):621–629, 2009.
- [20] Yu Yamashita, Junto Tsurumi, Masahiro Ohno, Ryo Fujimoto, Shohei Kumagai, Tadanori Kurosawa, Toshihiro Okamoto, Jun Takeya, and Shun Watanabe. Efficient molecular doping of polymeric semiconductors driven by anion exchange. *Nature*, 572(7771):634–638, 2019.
- [21] Hitoshi Kato, Susumu Takemura, and Yasushi Nakajima. Xps/ups studies of conducting polymers: exchange doping of dye molecules into polymer matrix. *Thin Solid Films*, 317(1):367–370, 1998.
- [22] Rui-Qi Png, Mervin CY Ang, Meng-How Teo, Kim-Kian Choo, Cindy Guanyu Tang, Dagmawi Belaineh, Lay-Lay Chua, and Peter KH Ho. Madelung and hubbard interactions in polaron band model of doped organic semiconductors. *Nature communications*, 7(1):1–9, 2016.
- [23] Shu-Jen Wang, Deepak Venkateshvaran, M. R. Mahani, Uday Chopra, Erik R. McNellis, Riccardo Di Pietro, Sam Schott, Angela Wittmann, Guillaume Schweicher, Murat Cubukcu, Keehoon Kang, Remington Carey, Thomas J. Wagner, Janis N. M. Siebrecht, Daniel P. G. H. Wong, Ian E. Jacobs, Razan O. Aboljadayel, Adrian Ionescu, Sergei A. Egorov, Sebastian Mueller, Olga Zadvorna, Piotr Skalski, Cameron Jellett, Mark Little, Adam Marks, Iain McCulloch, Joerg Wunderlich, Jairo Sinova, and Henning Sirringhaus. Long spin diffusion lengths in doped conjugated polymers due to enhanced exchange coupling. *Nature Electronics*, 2(3):98–107, 2019.
- [24] Chi Yueh Kao, Bumsu Lee, Leszek S. Wielunski, Martin Heeney, Iain McCulloch, Eric Garfunkel, Leonard C. Feldman, and Vitaly Podzorov. Doping of conjugated polythiophenes with alkyl silanes. *Advanced Functional Materials*, 19(12):1906–1911, 2021/04/16 2009.
- [25] Shrayesh N. Patel, Anne M. Glauddell, David Kiefer, and Michael L. Chabinc. Increasing the thermoelectric power factor of a semiconducting polymer by doping from the vapor phase. *ACS Macro Letters*, 5(3):268–272, 03 2016.
- [26] Friedrich G Helfferich. *Ion exchange*. Courier Corporation, 1995.
- [27] Ian E. Jacobs, Erik W. Aasen, Julia L. Oliveira, Tayane N. Fonseca, John D. Roehling, Jun Li, Guangwu Zhang, Matthew P. Augustine, Mark Mascal, and Adam J. Moule. Comparison of solution-mixed and sequentially processed p3ht:f4tcnq films: Effect of doping-induced aggregation on film morphology. *Journal of Materials Chemistry C*, 4(16):3454–3466, 2016.
- [28] Jun Li, Correy Koshnick, Souleymane O. Diallo, Sophia Ackling, David M. Huang, Ian E. Jacobs, Thomas F. Harrelson, Kunlun Hong, Guangwu Zhang, Joseph Beckett, Mark Mascal, and Adam J. Moulé. Quantitative measurements of the temperature-dependent microscopic and macroscopic dynamics of a molecular dopant in a conjugated polymer. *Macromolecules*, 50(14):5476–5489, 07 2017.
- [29] John H. Burke and Matthew J. Bird. Energetics and escape of interchain-delocalized ion

- pairs in nonpolar media. *Advanced Materials*, 31(12):1806863, 2020/05/21 2019.
- [30] Cheng Zhong, Yida Deng, Wenbin Hu, Jinli Qiao, Lei Zhang, and JiuJun Zhang. A review of electrolyte materials and compositions for electrochemical supercapacitors. *Chemical Society Reviews*, 44(21):7484–7539, 2015.
- [31] Wanxiang Zhao and Jianwei Sun. Triflimide (hntf2) in organic synthesis. *Chemical Reviews*, 118(20):10349–10392, 10 2018.
- [32] Tucker L. Murrey, Margaret A. Riley, Goktug Gonel, Dexter D. Antonio, Leah Filardi, Nikolay Shevchenko, Mark Mascal, and Adam J. Moulé. Anion exchange doping: Tuning equilibrium to increase doping efficiency in semiconducting polymers. *The Journal of Physical Chemistry Letters*, 12(4):1284–1289, 02 2021.
- [33] G. J. Brealey and Norbert Uri. Photochemical oxidation-reduction and photocatalysis. the photochemical activity of fecl_4^- in alcohol as oxidizing agent and as catalyst. *The Journal of Chemical Physics*, 20(2):257–262, 2020/11/11 1952.
- [34] Terry B. Swanson and Victor W. Laurie. Electron magnetic resonance and electronic spectra of tetrachloroferrate(iii) ion in nonaqueous solution. *The Journal of Physical Chemistry*, 69(1):244–250, 01 1965.
- [35] Maciej Galiński, Andrzej Lewandowski, and Izabela Stepniak. Ionic liquids as electrolytes. *Electrochimica Acta*, 51(26):5567–5580, 2006.
- [36] Byron. Kratochvil and Robert. Long. Iron(iii)-(ii) couple in acetonitrile. oxidation of thiocyanate by iron(iii). *Analytical Chemistry*, 42(1):43–46, 01 1970.
- [37] Mauro Magini and Tamas Radnai. X-ray diffraction study of ferric chloride solutions and hydrated melt. analysis of the iron (iii)-chloride complexes formation. *The Journal of Chemical Physics*, 71(11):4255–4262, 2020/06/19 1979.
- [38] Weihua Liu, Barbara Etschmann, Joël Brugger, Leone Spiccia, Garry Foran, and Brent McInnes. Uv-vis spectrophotometric and xafs studies of ferric chloride complexes in hypersaline licl solutions at 25–90 °c. *Chemical Geology*, 231(4):326–349, 2006.
- [39] Zhiming Liang, Yadong Zhang, Maryam Souri, Xuyi Luo, Alex M. Boehm, Ruipeng Li, Yan Zhang, Tairan Wang, Doo-Young Kim, Jianguo Mei, Seth R. Marder, and Kenneth R. Graham. Influence of dopant size and electron affinity on the electrical conductivity and thermoelectric properties of a series of conjugated polymers. *Journal of Materials Chemistry A*, 6(34):16495–16505, 2018.
- [40] Yoichi Shimura and Ryutaro Tsuchida. Absorption spectra of co (iii) complexes. ii. redetermination of the spectrochemical series. *Bulletin of the Chemical Society of Japan*, 29(3):311–316, 1956.
- [41] Donald O. Whittemore and Donald Langmuir. Standard electrode potential of $\text{fe}^{3+} + \text{e}^- = \text{fe}^{2+}$ from 5–35.deg. *Journal of Chemical & Engineering Data*, 17(3):288–290, 07 1972.
- [42] Sergio Trasatti. The absolute electrode potential: an explanatory note. *Pure Appl. Chem*, 58(7):955–966, 1986.
- [43] Claudia M. Cardona, Wei Li, Angel E. Kaifer, David Stockdale, and Guillermo C. Bazan. Electrochemical considerations for determining absolute frontier orbital energy levels of conjugated polymers for solar cell applications. *Advanced Materials*, 23(20):2367–2371, 2020/07/13 2011.
- [44] Robert R Gagne, Carl A Koval, and George C Lisensky. Ferrocene as an internal standard for electrochemical measurements. *Inorganic Chemistry*, 19(9):2854–2855, 1980.
- [45] Yevhen Karpov, Tim Erdmann, Ivan Raguzin, Mahmoud Al-Hussein, Marcus Binner, Uwe Lappan, Manfred Stamm, Kirill L. Gerasimov, Tetyana Beryozkina, Vasiliy Bakulev, Denis V. Anokhin, Dimitri A. Ivanov, Florian Günther, Sibylle Gemming, Gotthard Seifert, Brigitte Voit, Riccardo Di Pietro, and Anton Kiri. High conductivity in molecularly p-doped diketopyrrolopyrrole-based polymer: The impact of a high dopant strength and good structural order. *Advanced Materials*, 28(28):6003–6010, 2016.
- [46] Marija Bešter-Rogač, Alexander Stoppa, and Richard Buchner. Ion association of imidazolium ionic liquids in acetonitrile. *The Journal of Physical Chemistry B*, 118(5):1426–1435, 02 2014.

- [47] Hisaaki Tanaka, Satoshi Nishio, Hiroshi Ito, and Shin-ichi Kuroda. Microscopic signature of insulator-to-metal transition in highly doped semicrystalline conducting polymers in ionic-liquid-gated transistors. *Applied Physics Letters*, 107(24):243302, 2020/06/25 2015.
- [48] Jean Luc Bredas and G. Bryan Street. Polarons, bipolarons, and solitons in conducting polymers. *Accounts of Chemical Research*, 18(10):309–315, 10 1985.
- [49] Raja Ghosh and Frank C. Spano. Excitons and polarons in organic materials. *Accounts of Chemical Research*, 53(10):2201–2211, 10 2020.
- [50] Connor G. Bischak, Lucas Q. Flagg, Kangrong Yan, Tahir Rehman, Daniel W. Davies, Ram-sess J. Quezada, Jonathan W. Onorato, Christine K. Luscombe, Ying Diao, Chang-Zhi Li, and David S. Ginger. A reversible structural phase transition by electrochemically-driven ion injection into a conjugated polymer. *Journal of the American Chemical Society*, 142(16):7434–7442, 04 2020.
- [51] R. Joseph Kline, Dean M. DeLongchamp, Daniel A. Fischer, Eric K. Lin, Lee J. Richter, Michael L. Chabiny, Michael F. Toney, Martin Heeney, and Iain McCulloch. Critical role of side-chain attachment density on the order and device performance of polythiophenes. *Macromolecules*, 40(22):7960–7965, 10 2007.
- [52] Neil G. Connelly and William E. Geiger. Chemical redox agents for organometallic chemistry. *Chemical Reviews*, 96(2):877–910, 01 1996.
- [53] Iain McCulloch, Martin Heeney, Clare Bailey, Kristijonas Genevicius, Iain MacDonald, Maxim Shkunov, David Sparrowe, Steve Tierney, Robert Wagner, Weimin Zhang, Michael L. Chabiny, R. Joseph Kline, Michael D. McGehee, and Michael F. Toney. Liquid-crystalline semiconducting polymers with high charge-carrier mobility. *Nature Materials*, 5(4):328–333, 2006.
- [54] Y. Karpov, N. Kiri, M. Al-Hussein, M. Hamsch, T. Beryozkina, V. Bakulev, S. C. B. Mannsfeld, B. Voit, and A. Kiri. Hexacyano-[3]-radialene anion-radical salts: a promising family of highly soluble p-dopants. *Chemical Communications*, 54(3):307–310, 2018.
- [55] Phillip K. Koech, Asanga B. Padmaperuma, Liang Wang, James S. Swensen, Evgueni Polikarpov, Jens T. Darsell, James E. Rainbolt, and Daniel J. Gaspar. Synthesis and application of 1,3,4,5,7,8-hexafluorotetracyanonaphthoquinodimethane (f6-tnap): A conductivity dopant for organic light-emitting devices. *Chemistry of Materials*, 22(13):3926–3932, 07 2010.
- [56] A Davison, N Edelstein, RH Holm, and AH Maki. Synthetic and electron spin resonance studies of six-coordinate complexes related by electron-transfer reactions. *Journal of the American Chemical Society*, 86(14):2799–2805, 1964.
- [57] Sergio A. Paniagua, Jose Baltazar, Hossein Sojoudi, Swagat K. Mohapatra, Siyuan Zhang, Clifford L. Henderson, Samuel Graham, Stephen Barlow, and Seth R. Marder. Production of heavily n- and p-doped cvd graphene with solution-processed redox-active metal-organic species. *Mater. Horiz.*, 1:111–115, 2014.
- [58] Tadamichi Fukunaga. Negatively substituted trimethylenecyclopropane dianions. *Journal of the American Chemical Society*, 98(2):610–611, 01 1976.
- [59] Ronald Chwang, B. J. Smith, and C. R. Crowell. Contact size effects on the van der pauw method for resistivity and hall coefficient measurement. *Solid-State Electronics*, 17(12):1217–1227, 1974.
- [60] Daniel W. Koon. Effect of contact size and placement, and of resistive inhomogeneities on van der pauw measurements. *Review of Scientific Instruments*, 60(2):271–274, 2020/12/01 1989.
- [61] Nanoscale Device Characterization Division NIST Physical Measurement Laboratory. Resistivity and hall measurements. www.nist.gov/pml/nanoscale-device-characterization-division/popular-links/hall-effect/resistivity-and-hall.
- [62] Abraham. Savitzky and M. J. E. Golay. Smoothing and differentiation of data by simplified least squares procedures. *Analytical Chemistry*, 36(8):1627–1639, 07 1964.
- [63] Zhang Jiang. *GIXSGUI*: a MATLAB toolbox for grazing-incidence X-ray scattering data visualization and reduction, and indexing of buried

three-dimensional periodic nanostructured films.
Journal of Applied Crystallography, 48(3):917–
926, Jun 2015.

- [64] Jonathan Rivnay, Rodrigo Noriega, R. Joseph Kline, Alberto Salleo, and Michael F. Toney. Quantitative analysis of lattice disorder and crystallite size in organic semiconductor thin films. *Phys. Rev. B*, 84:045203, Jul 2011.